ISSN 1674-1056
http://cpb.iphy.ac.cn
http://iopscience.iop.org/cpb
中国物理 B
Chinese Physics
中国物理 Chinese Physics B

Thermal transport in semiconductor nanostructures, graphene, and related two-dimensional materials

Alexandr I. Cocemasov, Calina I. Isacova, Denis L. Nika
Citation: Chin. Phys. B . 2018, 27(5): 056301. **doi:** 10.1088/1674-1056/27/5/056301

Journal homepage: http://cpb.iphy.ac.cn; http://iopscience.iop.org/cpb

What follows is a list of articles you may be interested in

Thermal transport in twisted few-layer graphene

Min-Hua Wang(王敏华), Yue-E Xie(谢月娥), Yuan-Ping Chen(陈元平)
Chin. Phys. B . 2017, 26(11): 116503. **doi:** 10.1088/1674-1056/26/11/116503

Temperature-induced effect on refractive index of graphene based on coated in-fiber Mach-Zehnder interferometer

Li-Jun Li(李丽君), Shun-Shun Gong(宫顺顺), Yi-Lin Liu(刘仪琳), Lin Xu(徐琳), Wen-Xian Li(李文宪), Qian Ma(马茜), Xiao-Zhe Ding(丁小哲), Xiao-Li Guo(郭晓丽)
Chin. Phys. B . 2017, 26(11): 116504. **doi:** 10.1088/1674-1056/26/11/116504

Thermal conductivity of carbon nanoring linked graphene sheets:A molecular dynamics investigation

Gang Shi(石刚), Jianwei Zhang(张鉴炜), Yonglv He(贺雍律), Su Ju(鞠苏), Dazhi Jiang(江大志)
Chin. Phys. B . 2017, 26(10): 106502. **doi:** 10.1088/1674-1056/26/10/106502

Structural and optical properties of thermally reduced graphene oxide for energy devices

Ayesha Jamil, Faiza Mustafa, Samia Aslam, Usman Arshad, Muhammad Ashfaq Ahmad
Chin. Phys. B . 2017, 26(8): 086501. **doi:** 10.1088/1674-1056/26/8/086501

Lattice vibration and thermodynamical properties of a single-layergraphene in the presence of vacancy defects

Sha Li(黎莎), Zeng-Tao Lv(吕增涛)
Chin. Phys. B . 2017, 26(3): 036303. **doi:** 10.1088/1674-1056/26/3/036303

TOPICAL REVIEW — Thermal and thermoelectric properties of nano materials

Thermal transport in semiconductor nanostructures, graphene, and related two-dimensional materials*

Alexandr I. Cocemasov, Calina I. Isacova, and Denis L. Nika†

E. Pokatilov Laboratory of Physics and Engineering of Nanomaterials, Department of Physics and Engineering, Moldova State University, Chisinau MD-2009, Republic of Moldova

(Received 13 February 2018; revised manuscript received 15 March 2018; published online 26 April 2018)

We review experimental and theoretical results on thermal transport in semiconductor nanostructures (multilayer thin films, core/shell and segmented nanowires), single- and few-layer graphene, hexagonal boron nitride, molybdenum disulfide, and black phosphorus. Different possibilities of phonon engineering for optimization of electrical and heat conductions are discussed. The role of the phonon energy spectra modification on the thermal conductivity in semiconductor nanostructures is revealed. The dependence of thermal conductivity in graphene and related two-dimensional (2D) materials on temperature, flake size, defect concentration, edge roughness, and strain is analyzed.

Keywords: phonons, thermal conductivity, nanowire, graphene, two-dimensional (2D) materials

PACS: 63.22.Rc, 63.22.–m, 65.80.Ck, 65.80.–g **DOI:** 10.1088/1674-1056/27/5/056301

1. Thermal transport in semiconductor nanostructures

Rapid miniaturization of electronic devices to nanoscale range requires new approaches for efficient management of their heat and electrical conductions. One of these approaches, referred to as phonon engineering,[1] is related to optimization of thermal and electronic properties of nanodimensional structures via modification of their phonon properties.[1–3] At the end of the previous century, several research groups have demonstrated that many phonon confined branches appear in energy spectra of homogeneous semiconductor thin films and nanowires,[4–9] leading to change in phonon density of states (PDOS) and reduction of average phonon group velocity in comparison with the corresponding bulk materials.[7–9] The latter together with enhanced phonon boundary scattering results in decreasing of lattice thermal conductivity (TC). Balandin and Wang[7] have theoretically predicted that the lattice thermal conductivity of 10-nm-thick silicon film is by an order of magnitude smaller than that in bulk silicon at room temperature (RT). Five-times drop of lattice thermal conductivity was also theoretically predicted for Si nanowire with a diameter of 20 nm.[10] Subsequent independent theoretical studies[11–17] and experimental measurements of thermal conductivity in several nm-thick free-standing Si films, nanowires, and nanotubes[18–23] confirmed the initial predictions: strong reduction of lattice thermal conductivity as compared with that of bulk material.

More precise tuning of phonon properties and heat conduction at nanoscale can be realized in multilayer films (MFs) and core/shell nanowires (NWs).[24–35] The evolution of phonon energies in homogeneous silicon films and silicon films covered by diamond claddings is illustrated in Fig. 1, where we show the dispersion relations for the dilatation (SA) phonon modes in (a) the free-standing Si film; (b)–(c) diamond/Si/diamond heterostructures with different thicknesses of the diamond (D) barrier layer; and (d) the Si film with the clamped external surfaces, which corresponds to a film embedded in the "absolutely" rigid material. The thickness of the Si layer in all cases is 2 nm to insure the strong phonon confinement effect at RT. The phonon energies for each phonon branch s in the free-standing film are lower than those in the clamped film. Phonon modes of the D/Si/D heterostructure occupy an intermediate position between the two limiting cases depending on the diamond layer thickness.

Modification of phonon energy spectra and phonon density of states in MFs and core/shell NWs leads to significant change in average phonon group velocity $\bar{v}^{(\alpha)}$, where α denotes the phonon polarization. The dependence of $\bar{v}^{(\alpha)}$ on the phonon frequency for dilatation phonon modes in bare GaN nanowire, GaN/AlN and GaN/plastic core/shell nanowires is presented in Fig. 2. The average group velocity curves $\bar{v}(\omega)$ are strongly oscillating functions due to the presence of many quantized phonon branches s and the fast variation of the derivatives $1/v_s^{(\alpha)}(\omega)) = \mathrm{d}q_s^{(\alpha)}(\omega)/\mathrm{d}\omega$ with changing ω. The acoustically soft and slow plastic shell decreases the phonon group velocity by a factor of 3 in comparison with bare GaN NW, while the acoustically hard and fast AlN shell leads to an opposite effect of increasing $\bar{v}^{(\alpha)}$ by a factor of 1.3.[26]

*Project supported by the Republic of Moldova through the projects 15.817.02.29F and 17.80013.16.02.04/Ua.

†Corresponding author. E-mail: dlnika@yahoo.com

© 2018 Chinese Physical Society and IOP Publishing Ltd

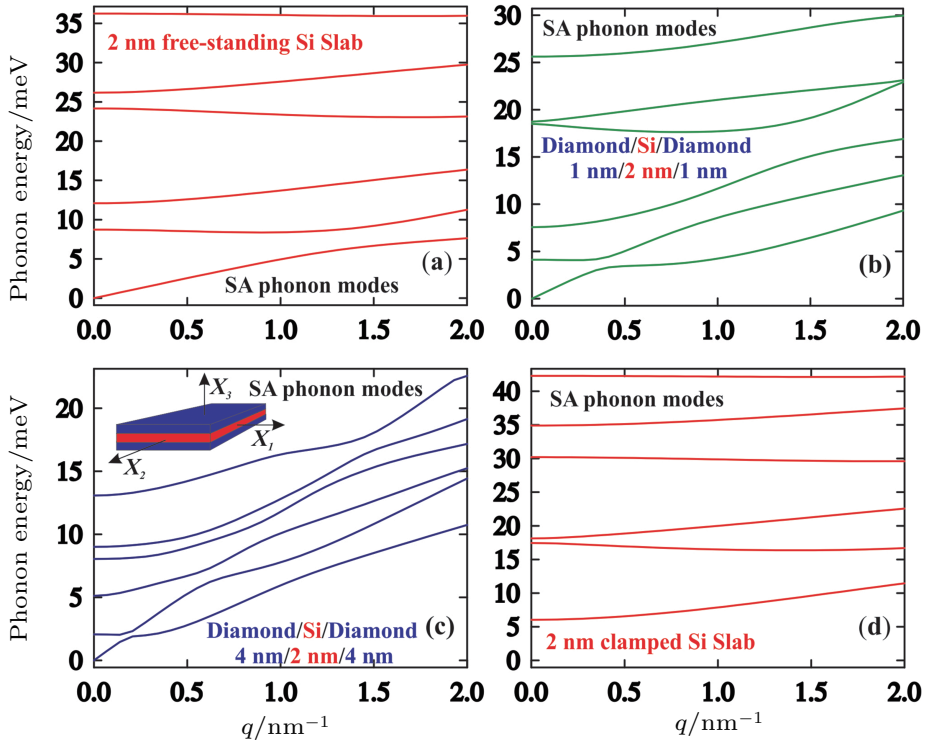


Fig. 1. (color online) Energy dispersions of the dilatational (SA) acoustic phonons in 2-nm thick free-standing Si slab (a), diamond/Si/diamond heterostructures with dimensions 1 nm/2 nm/1 nm (b) and 4 nm/2 nm/4 nm (c), and 2-nm thick Si slab with clamped boundaries (d). Reprinted with permission from Ref. [27] (copyright 2008 American Institute of Physics).

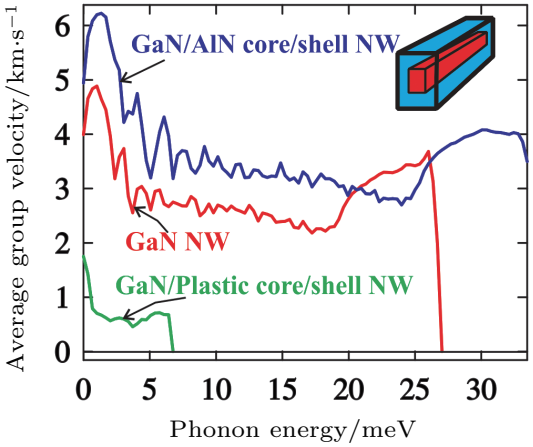


Fig. 2. (color online) Average phonon group velocity as a function of the phonon frequency for dilatational modes in rectangular GaN, GaN/AlN, and GaN/plastic nanowires. Reprinted with permission from Ref. [26] (copyright 2005 American Physical Society).

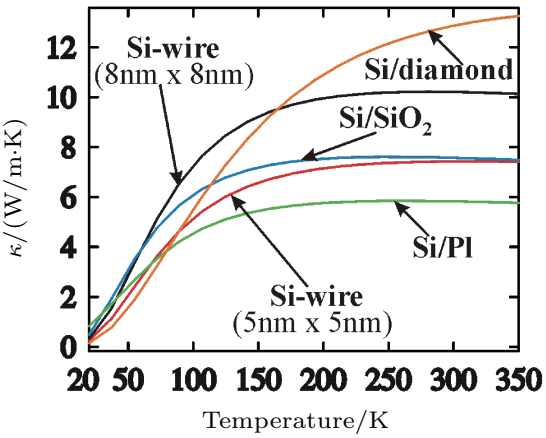


Fig. 3. (color online) Temperature dependence of phonon thermal conductivity in Si nanowires and Si/SiO_2, Si/Pl, and Si/diamond core/shell nanowires.

The effect of shell layers on thermal conductivity of Si film is illustrated in Fig. 3, where temperature dependence of thermal conductivity is shown for bare Si NW and core/shell Si/diamond, Si/plastic, and Si/SiO_2 NWs. The diamond shell with higher sound velocity than that in Si increases the thermal conductivity in the core/shell NWs in comparison with Si NW at temperatures $T > 150$ K. The plastic and SiO_2 shells (with low sound velocity) suppress heat propagation in the core/shell nanowires. Change in the thermal conductivity is primarily induced by the mixing of phonons from the core and the shell, leading to appearance of hybrid phonon modes which propagate through the whole core/shell nanowire.

Segmented nanowires consisted of segments of different materials and shapes were recently proposed as efficient phonon filters, removing many phonon modes from the heat flux due to their trapping in nanowire segments.[17,29,32,35] Figure 4 presents the temperature dependence of phonon thermal conductivity for Si NW, segmented cross-section modulated Si NW (SMNW), and segmented cross-section modulated Si/Ge core/shell nanowires. Increasing the thickness of the Ge shell from 1 ML to 7 ML leads to a decrease of thermal conductivity of Si/Ge SMNW by a factor of 2.9–4.8 in comparison with that in Si SMNW without Ge shell, and by a factor of 13–38 in comparison with that in bare Si NW. The reduction in κ of Si/Ge segmented cross-section modulated NWs is substantially stronger than that reported for the core/shell

nanowires without cross-sectional modulation.[16,30,31,33] In core/shell nanowires without modulation, the drop of thermal conductivity occurs mainly due to hybridization of phonon modes, resulting in changes of PDOS and phonon relaxation. In SMNWs, reduction of lattice thermal conductivity is reinforced due to interplay between hybridization of phonon modes and their localization in NW segments, which completely removes such modes from the heat flux.[35]

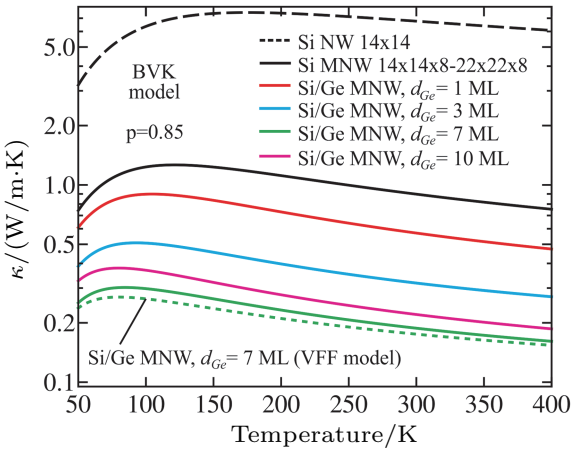


Fig. 4. (color online) Phonon thermal conductivity as a function of the absolute temperature. Results are presented for Si NW, Si SMNW, and core/shell Si/Ge SMNWs with different thicknesses of Ge. Reprinted with permission from Ref. [35] (copyright 2013 American Institute of Physics).

Spatial confinement of phonons in nanostructures opens up new possibilities for engineering electron–phonon interaction and electron mobility. Formation of electron and phonon minibands in nanostructures with energy gaps between the confined branches may result in phonon bottleneck effect,[36–38] non-monotonic (oscillated) dependence of electron mobility on nanostructure thickness,[39–42] suppression of electron–phonon scattering at certain electron energies, and enhancement of electron mobility.[27,43–45] Nika *et al.*[27] and Fonoberov *et al.*[45] showed theoretically that RT electron mobility in Si thin films or Si nanowires with diamond barrier layers is by a factor of 2–4 higher than that in bare Si films or NWs. The enhancement effect was explained by strong modification of phonon energy spectra inside the Si channel layer, leading to reduction of electron-phonon scattering.[27,45]

Although the appearance of confined phonon energy branches in semiconductor nanostructures has been predicted theoretically by many research groups[4–17,24–29] and has been indirectly confirmed by thermal conductivity measurements,[18–23] direct observation of confined acoustic phonon modes was made very recently, using Brillouin–Mandelstam light scattering spectroscopy.[46] Figure 5 shows the acoustic phonon energy branches in GaAs nanowires with diameter of 122 nm. Solid lines are calculated in the framework of elastic continuum approach, while open dots represent experimental phonon energies measured using Brillouin–Mandelstam spectrometer. Confined phonon energy branches separated by energy gaps are clearly seen in Fig. 5.

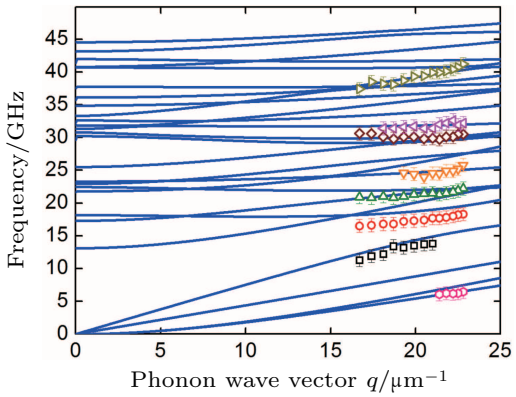


Fig. 5. (color online) Measured and calculated phonon dispersions for a GaAs nanowire with diameter of 122 nm along [111] direction. Reprinted with permission from Ref. [46] (copyright 2016 Nature Publishing Group).

2. Thermal transport in single-layer graphene

Monoatomic sheet of sp^2-hybridized carbon atoms, graphene, demonstrates unique electrical,[47,48] optical,[49,50] and thermal[51–54] properties owing to quasi two-dimensional electron and heat propagation. Extremely high thermal conductivity[51–54] and electron mobility[55,56] make graphene a promising material for heat-removal applications and electronics. First experimental measurements of thermal conductivity in suspended single-layer graphene (SLG) flakes were performed using Raman optothermal method developed by Balandin and co-workers.[51,54] In this method, laser light was used for heating up graphene flakes suspended over trench, while the temperature rise was extracted from the shift of the Raman G-band. The ultra-high values of RT thermal conductivity $\kappa \sim 3000$–5000 W/m·K were measured in rectangular graphene flakes with dimensions 5 μm×10 μm.[51,54] These values are by an order of magnitude higher than that of cuprum or aurum and by a factor of 2–3 higher than that of bulk diamond or highly-oriented pyrolytic graphite. Significant experimental and theoretical efforts have been made later to investigate peculiarities of phonon modes and thermal transport in graphene and graphene nanoribbons.[57–82] The thermal conductivity of suspended graphene in the range of 1600–3800 W/m·K at temperatures close to the RT was measured using different experimental techniques: Raman optothermal[57–60] or electrical self-heating[61] methods. Different theoretical models were employed for the investigation of two-dimensional phonon transport in graphene: Boltzmann-transport equation (BTE) approach,[63–70,75–77] equilibrium and non-equilibrium molecular dynamics.[73,74,78–80] Strong dependence of thermal conductivity on temperature, flake size and shape, strain, edge quality, and crystal lattice defects was predicted in numerous

theoretical studies.[63–81] The phonon mean free path (MFP) in high-quality suspended graphene was estimated to be as long as 800 nm at RT.[54] Therefore, the thermal conductivity is very sensitive to both intrinsic and extrinsic phonon scatterings. The latter is crucial for the engineering of phonon and thermal properties of graphene. The dependence of lattice thermal conductivity in singe-layer graphene on temperature and flake width d is illustrated in Fig. 6(a). The average experimental value of TC reported in Refs. [51] and [54] is also shown as a purple dot for comparison. The theoretical curves were calculated in the framework of BTE approach taking into account three-phonon Umklapp and edge roughness scatterings. The thermal conductivity decreases with temperature rise due to enhancement of three-phonon Umklapp scattering. However, even at $T = 400$ K, the influence of the flake width on κ is very pronounced: decreasing d from 9 μm to 3 μm results in two-fold reduction of thermal conductivity. At the same time, the four-phonon scattering limits MFP of low-energy phonons, removing the dependence of κ on flake length L for $L > 100$ μm[69] and may decrease the lattice thermal conductivity.[82] Dependence of RT TC on defect concentration induced by electron beam irradiation is presented in Fig. 6(b). Solid curves correspond to theoretical results calculated using the BTE with different values of specularity parameter p. The experimental data are shown in Fig. 6(b) by squares, circles, and triangles. For the small defect densities $N_D < 1.2 \times 10^{11}$ cm^{-2}, the thermal conductivity rapidly decreases with N_D. At higher defect density, the thermal conductivity reveals weakening of the $\kappa(N_D)$ dependence, which is explained theoretically by the interplay between the three main phonon scattering mechanisms: Umklapp scattering due to lattice anharmonicity, mass-difference scattering, and rough edge scattering.[80]

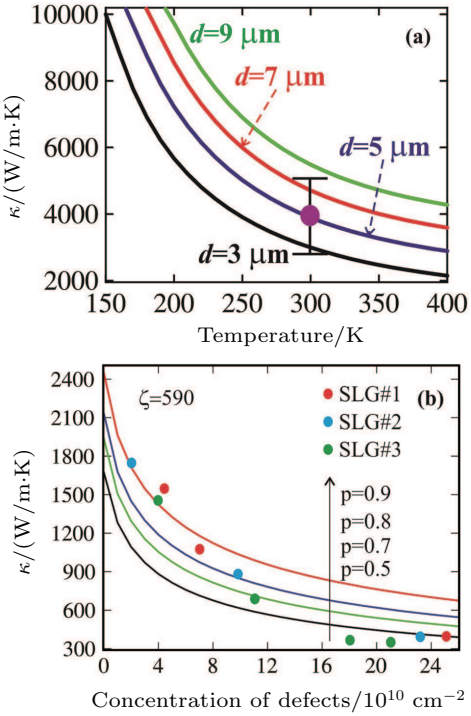


Fig. 6. (color online) (a) Thermal conductivity of graphene as a function of temperature shown for different graphene flake widths. The results were calculated for the specularity parameter $p = 0.9$. An experimental data point (purple dot) from Refs. [51] and [54] is also shown for comparison. (b) Thermal conductivity of graphene as a function of the density of defects induced by electron beam irradiation. The experimental results are shown by circle points. The solid curves correspond to the BTE results, plotted for different values of specularity parameter p. Adopted with permission from Ref. [63] (copyright 2009 American Physical Society) and from Ref. [80] (copyright 2016 The Royal Society of Chemistry).

Table 1. Thermal conductivity of single-layer graphene: experimental data.

κ/(W/m·K)	Method	Brief description	Ref.
~ 3000–5000		suspended; exfoliated; $T \sim 300$ K	[51], [54]
2500		suspended; chemical vapor deposition (CVD) grown; $T \sim 300$ K	[57]
1500–5000	Raman optothermal	suspended; CVD grown	[58]
1600–2800		suspended; strong isotope dependence; $T \sim 380$ K	[59]
2778.3 ± 569		suspended, $T \sim 325$ K	[60]
2000–3800	electrical self-heating	exfoliated and CVD grown; $T \sim 300$ K	[61]
600	electrical	supported; exfoliated	[62]

Table 2. Thermal conductivity of single-layer graphene: theoretical data.

Brief description	Refs.
Strong dependence of TC on flake size	[63]–[74]
Strong dependence of TC on strain	[75]–[77]
Strong dependence of TC on point defects	[73], [75], [76], [78], [79]
Strong dependence of TC on isotopes	[75], [76], [80]
Strong dependence of TC on edge roughness	[63], [69], [79], [81]

Thermal conductivity of graphene supported on a substrate[62] or graphene encased within cladding layers[83] is several times smaller than that of suspended graphene due to phonon scattering on interfaces between graphene and substrate/cladding layers and modification of graphene phonon modes. The experimental and theoretical data on the thermal conductivity of single-layer graphene are summarized in Tables 1 and 2. Readers interested in more detailed description of phonon modes and thermal transport in graphene are referred to different reviews.[2,52,53,84–89] Application of Raman optothermal method for the thermal conductivity measurements in graphene and related two-dimensional materials is comprehensively described in the recent review by Malekpour and Balandin.[90] Accuracy and limitations of

Raman-optothermal method as well as its modifications are discussed in Refs. [91]–[95].

3. Thermal transport in few-layer graphene

Several interesting results have been obtained in the field of thermal transport in few-layer graphene (FLG) during the last few years.[91,96–110] A series of independent measurements of thermal conductivity in FLG has been performed.[91,96–98] Ghosh *et al.*[91] reported on the measurements of thickness-dependent thermal conductivity in FLG. Rapid decrease of TC with increase of number of layers from 1 up to 4 was observed and explained theoretically by increase in phase space allowed for three-phonon Umklapp scattering.[91] Jo *et al.*[96] measured the TC in exfoliated and suspended bilayer graphene (BLG) samples using electro-thermal micro-bridge method and found TC in the range (730–880)± 60 W/m·K at RT. These values are 2–3 times lower than those obtained using Raman optothermal technique,[60,91] while in accordance with previous electro-thermal measurements.[99–101] It was argued that this suppression is mainly caused by scattering from polymer residues on the graphene surface. Li *et al.*[60] employed Raman optothermal technique for investigation of thermal transport in twisted bilayer graphene (T-BLG). The authors found that in the wide range of temperatures 300–750 K, the TC in T-BLG is smaller than that in both SLG and AB-BLG (see Fig. 7(a)). The thermal conductivity of T-BLG is by a factor of ~ 2 smaller than that in SLG and by a factor of ~ 1.35 smaller than that in AB-BLG near the RT. The drop of TC was explained by emergence of many additional hybrid folded phonons in T-BLG, resulting in more intensive phonon scattering.[60,102–104] Jeong *et al.*[97] reported the TC of 2868 ± 932 W/m·K at RT for CVD large-scale free-standing FLG in which a micropipette temperature sensor with an inbuilt laser point heating source was used. The large uncertainty of 32% in TC measurement was attributed mainly to the non-uniform thickness of the film in the range 1–10 layers with an average thickness around 7 layers. The layer numbers were determined from the intensity ratio of Raman G-band to 2D-band and full width at half maximum of the 2D-band. Liu *et al.*[98] measured the TC at RT of millimeter-size CVD FLG supported on organic substrate (PMMA) in the range 33–365 W/m·K depending on the FLG thickness, using the transient electro-thermal technique. The mm-scale of the sample eliminated the thermal contact resistance problems and phonon–edge scattering encountered in μm-scale samples. The obtained values are about one order of magnitude lower than that of suspended graphene and are significantly lower than TC of supported graphene on SiO_2. The authors assumed that the abundant C atoms in the PMMA enhance the energy and momentum exchange with the supported graphene, thus reinforcing the phonon scattering and reducing the TC of CVD graphene on PMMA in comparison with SiO_2 substrate.

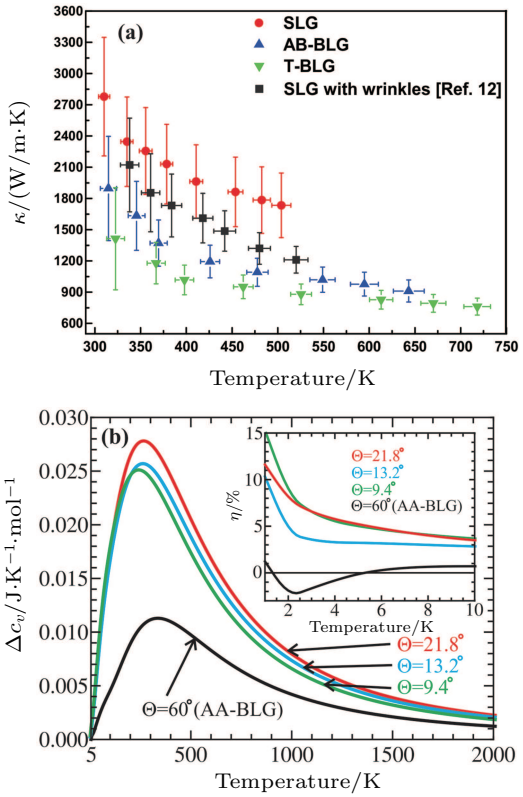


Fig. 7. (color online) (a) Thermal conductivity of suspended SLG, AB-BLG, and T-BLG as a function of the measured temperature. (b) Dependence of the difference of the specific heat in T-BLG from that in AB-BLG on the temperature. The inset shows the relative difference between AB-BLG and T-BLG specific heats as a function of temperature. Reprinted with permission from Ref. [60] (copyright 2014 The Royal Society of Chemistry) and from Ref. [103] (copyright 2014 American Institute of Physics).

Nika *et al.*[103] and Cocemasov *et al.*[102,104] have theoretically demonstrated the possibility of phonon engineering of thermal properties of BLG and other 2D layered materials by twisting (rotating) the atomic planes. In these studies,[102–104] the calculations of phonon energy spectra in T-BLG were performed using the Born–von Karman model of lattice dynamics for intralayer atomic interactions and spherically symmetric interatomic potential for interlayer interactions. Nika *et al.*[103] revealed an intriguing dependence of the specific heat c_V in T-BLG on the rotational angle θ, which is particularly pronounced at low temperatures (see Fig. 7(b)). Specifically, the twisting decreases the specific heat in T-BLG by 10%–15% in comparison with AB-BLG at $T = 1$ K. Cocemasov *et al.*[104] within a more rigorous model, taking into account both anisotropy of phonon dispersions and non-parabolicity of ZA branch, showed that the low-temperature specific heat scales with temperature as $c_V \sim T^{1.3}$ for AB-BLG and $c_V \sim T^{1.6}$ for T-BLG with rotation angle $\theta = 21.8°$.

Limbu *et al.*[105] reported on the measurement of the RT TC of CVD synthesized polycrystalline T-BLG as a function

of grain size employing a noncontact optical technique based on micro-Raman spectroscopy. The measured TC values are 1305 ± 122 W/m·K, 971 ± 73 W/m·K, and 657 ± 42 W/m·K for average grain sizes of 54 nm, 21 nm, and 8 nm, respectively. The equilibrium molecular dynamics (EMD) simulations with reactive empirical bond order potential for covalent intralayer interaction and Lennard–Jones potential for interlayer interaction have also been employed.[105] The calculations revealed that the degradation in TC due to grain boundaries is smaller in a polycrystalline BLG than in polycrystalline SLG, which results from non-negligible interactions between adjacent graphene layers. Kuang *et al.*[106] calculated the RT TC of FLG up to four layers and graphite under different isotropic tensile strains in the framework of density functional theory (DFT) combined with phonon Boltzmann–Peierls equation. Enhancement of the intrinsic TC up to 40% was found both for FLG and graphite with strain amplification. It was concluded that this TC behavior is determined by competition between the decreased mode heat capacities and the increased lifetimes of flexural phonons. A similar TC behavior was observed for 2-layer hexagonal boron nitride systems. These results provide insights into engineering of the TC of FLG and related 2D layered materials by strain. Zhan *et al.*[107] investigated the thermal transport properties of BLG with interlayer linkages using the large-scale nonequilibrium molecular dynamics (NEMD) simulations and an adaptive intermolecular reactive empirical bond order potential. It was found that the BLG TC could be effectively tailored through the introduction of different types of interlayer linkages, i.e., divacancy bridgings, "spiro" interstitial bridgings, and Frenkel pair defects. The impacts from the interlayer linkages could be further modulated through their density and distribution. An up to 80% reduction in the TC was predicted for the BLG with 1.39% divacancy bridgings. It was also found that the linkages that contain vacancies (divacancy bridgings and Frenkel pair defects) lead to more severe suppression of the TC owing to a stronger phonon scattering. Shen *et al.*[108] studied the effects of number of graphene layers n and the size on TC of FLG embedded in an epoxy matrix. Their NEMD-based simulations showed that the in-plane TC of FLG and the TC across the FLG/epoxy interface simultaneously increase with increasing number of graphene layers. However, higher TC of FLG is not translated into higher TC of graphene/epoxy bulk composites unless they have large lateral sizes to maintain their aspect ratios comparable to the few-layer counterparts.[108] These findings signify the strong influence of FLG lateral sizes on its TC and offer a simple approach to effectively improving TCs of composites using FLG sheets.

Si *et al.*[109] employed the EMD simulations to study the effects of torsion on the TC of FLG. TC of 10-layer FLG with torsion angles of 0°, 11.25°, 22.5°, 33.75°, 45°, 67.5°, 90°, 112.5°, and 135° was calculated. The simulations revealed an intriguing dependence of the TC on torsion angles, namely, there is a minimum at torsion angle 22.5° with the lowest TC of 4692 W/m·K. The torsion effect was analyzed as a combination of the compression effect and the dislocation effect. The spectral energy density analysis showed that the effect of dislocation on TC can be negligible, while the compression effect decreases the phonon lifetimes of flexural ZA branches and increases the ZA group velocities and the phonon specific heat. The decrease dominates when the torsion angle is small, whereas the increase dominates at large torsion angles, which are responsible for the reported variation of TC. D'Souza and Mukherjee[110] reported on the calculation of the TC of SLG and BLG from DFT and BTE approach. An quantitative agreement with experimental data from Ref. [60] in the temperature range of 300–700 K has been achieved.

4. Thermal transport in related 2D layered materials

4.1. Hexagonal boron nitride

Hexagonal boron nitride (h-BN) holds many physical properties of practical importance such as high thermal conductivity, temperature stability, and excellent impermeability.[111] However, compared to graphene thermal research, there are much less experimental data for the TC of h-BN, although several interesting reports appeared in recent years.[112–114] Zhou *et al.*[113] measured the TC in suspended 9-layer h-BN sheets synthesized by a low pressure CVD method using the optothermal Raman technique. They found TC in the range 227–280 W/m·K at RT, which is close to the data previously reported for 5-layer h-BN[112] and comparable to that of bulk h-BN (∼ 390 W/m·K).[115] More recently, Wang *et al.*[114] provided experimental observation of the thickness-dependent TC in suspended few-layer h-BN similar to that of few-layer graphene. They found the RT TC of a suspended bilayer h-BN sample to be around 484 W/m·K, which clearly exceeds that of bulk h-BN, but smaller than theoretically predicted value of 520 W/m·K in single-layer h-BN.[116]

4.2. Molybdenum disulfide

Molybdenum disulfide (MoS_2), one of the transition metal dichalcogenides, has a natural thickness-dependent energy gap,[117,118] which makes it promising for electronic and optoelectronic applications. Recently, there appeared several experimental[119–121] and theoretical[122–125] studies on the thermal transport of single- and few-layer MoS_2. Yan *et al.*[119] reported on a Raman characterization of exfoliated and suspended single-layer MoS_2. The RT TC was found to be 34.5 ± 4 W/m·K, which is by a factor of 3 lower than that

of bulk MoS_2 [126] and by ~ 2 orders of magnitude lower than that of single-layer graphene.[51] A BTE-based calculation from the same work[119] agreed well with the measured value. Jo *et al.*[120] used the electro-thermal micro-bridge method to obtain the TC of suspended few-layer MoS_2 as a function of temperature. The measured RT TC values were 44–50 W/m·K and 48–52 W/m·K for 4- and 7-layer samples, respectively. In contrast to the suspended sample measurements, a relatively high TC of 62 W/m·K at RT was reported by Taube *et al.*[121] for supported single-layer MoS_2 using Raman optothermal technique. The authors suggested that the discrepancy may be associated with the different sample preparation and measurement conditions. Cai *et al.*[122] investigated the vibrational and thermal properties of single-layer MoS_2 using the density functional perturbation theory (DFPT). It was found that the dominated phonon mean free path is less than 20 nm, about 30-fold smaller than that of graphene. Combined with the nonequilibrium Green's function (NEGF) calculations, the RT TC around 23 W/m·K was predicted. Consistently, a value around 20 W/m·K of RT TC in single-layer MoS_2 was obtained by Ding *et al.*[123] based on NEMD simulations. In another study by the same authors,[124] the effects of lattice defects and mechanical strain on the TC of single-layer MoS_2 were investigated. It was predicted that a 0.5% concentration of mono-Mo vacancies is able to reduce the TC by about 60%. Moreover, a 12% tensile strain is able to reduce the TC by another 60%. A theoretical calculation by Gu *et al.*[125] based on phonon Boltzmann–Peierls equation approach has shown a decreasing trend in TC while going from 1- to 3-layer MoS_2 due to the changes in phonon dispersion relations and higher phonon scattering rates induced by the increased anharmonicity in few-layer MoS_2.

4.3. Black phosphorus

Single- and few-layer black phosphorus (phosphorene) is another promising 2D material for future electronics.[127–129] Due to its two distinct high-symmetry directions, denoted as zigzag (ZZ) and armchair (AC), phosphorene demonstrates anisotropic properties which could be useful for an efficient transport management. First theoretical studies of single-layer phosphorene thermal properties were carried out with NEGF[130] and BTE[131] approaches. TC values of 83.5 W/m·K and 24.3 W/m·K at RT along ZZ and AC directions with an anisotropy ratio ~ 3 were predicted in Ref. [131]. MD simulations of TC in single-layer phosphorene were performed in Ref. [132] and even larger anisotropy ratio ~ 5 along ZZ and AC directions was reported with RT TC values of 152.7 W/m·K and 33.0 W/m·K, respectively. Theoretical modeling in Ref. [133] revealed that the observed anisotropy is primarily related to the anisotropic phonon dispersion, whereas the intrinsic phonon scattering rates were found to be similar along the ZZ and AC directions. Hong *et al.*[134] predicted RT TC for infinite length ZZ and AC single-layer phosphorene to be 110.7 ± 1.75 W/m·K and 63.6 ± 3.9 W/m·K, respectively, using NEMD simulations. The thermal transport anisotropy was partially attributed to the direction-dependent phonon group velocities. Liu and Chang[135] employing BTE approach found that TC in single-layer phosphorene is a smoothly decreasing function of the crystal chirality while going from ZZ to AC directions (see Fig. 8). An unusually high contribution of 30% to the total TC from optical phonons was also predicted due to the group velocities and relaxation times comparable to those of acoustic phonons.

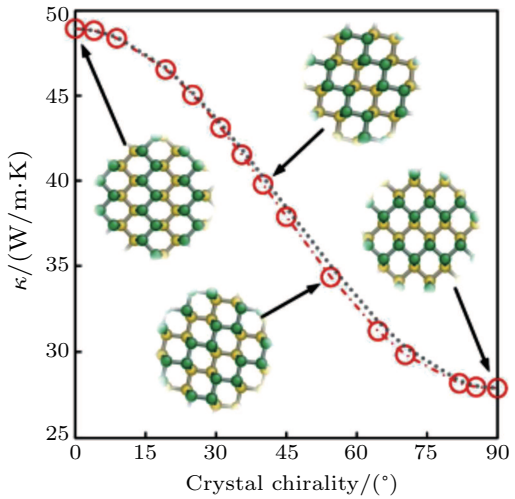


Fig. 8. (color online) Orientation-dependent thermal conductivity of 1 μm-length phosphorene sheet. The gray dot line is fitted by a cosine function with period 2π. The ZZ and AC chiralities correspond to 0° and 90°, respectively. Reproduced with permission from Ref. [135] (copyright 2015 The Royal Society of Chemistry).

Qin *et al.*[136] calculated the RT TC for single-layer phosphorene to be 30.15 W/m·K in ZZ direction and 13.65 W/m·K in AC direction in the framework of DFPT and BTE within relaxation time approximation approaches. The authors argued that the minor contribution around 5% of the ZA mode to the total TC is responsible for the low values of TC of phosphorene in comparison with graphene. In contrast, Jain and McGaughey[137] with a similar approach but without relaxation time approximation for the single-layer phosphorene predicted much higher TC values of 110 W/m·K and 36 W/m·K at RT along ZZ and AC directions with an anisotropy ratio of 3. The anisotropy was attributed to the anisotropic phonon dispersion, which leads to direction-dependent phonon group velocities. Zhang *et al.*[138] using NEMD simulations surprisingly found that TC of few-layer phosphorene (with in-plane dimensions 20 nm $\times$ 20 nm) is insensitive to the number of layers, which is in strong contrast to the thermal transport behavior in other 2D layered materials. This layer-independent TC is associated with the hindering of flexural phonon mode due to the puckered structure of phosphorene. The authors also predicted an increase

in the TC of phosphorene due to the tensile strain, in particular in the AC direction. Liu *et al.*[139] using NEMD simulations demonstrated the possibility to suppress the TC of phosphorene nanoribbons by structuring their edges. A significant reduction of $\sim 40\%$ in TC at RT was predicted in dimer- and tube-terminated phosphorene nanoribbons as compared to pristine phosphorene nanoribbons of the same width ~ 2 nm.

Recently, experimental reports on TC measurements in single- and few-layer phosphorene based on Raman optothermal,[133] time-domain thermoreflectance,[140,141] and four-probe[142,143] methods, appeared in the literature. The obtained TC values are in the same range as those predicted theoretically and generally correspond to the theoretical findings.

5. Conclusion

We have reviewed phonon and thermal properties of semiconductor nanostructures (multilayer films, core/shell and segmented nanowires), graphene, and related two-dimensional materials (hexagonal boron nitride, molybdenum disulfide, and black phosphorus). Controlled modification of phonon modes in semiconductor nanostructures opens up new possibilities for phonon-engineered optimization of electrical and heat transport. Unique features of quasi-two-dimensional phonon transport in graphene and related materials are discussed and comparative analysis of experimental and theoretical data on thermal conductivity in single-layer graphene, few-layer graphene, hexagonal boron nitride, molybdenum disulfide, and black phosphorus is provided.

Acknowledgment

DLN thanks Prof. Alexander A. Balandin (University of California, Riverside) for fruitful discussions of phonon and thermal phenomena in semiconductor nanostructures and graphene.

References

[1] Balandin A A 2005 *J. Nanosci. Nanotechnol.* **5** 1015
[2] Balandin A A and Nika D L 2012 *Materials Today* **15** 266
[3] Balandin A A, Pokatilov E P and Nika D L 2007 *J. Nanoel. Optoel.* **2** 140
[4] Bannov N, Mitin V and Stroscio M 1994 *Phys. Stat. Sol. (b)* **183** 131
[5] Bannov N, Aristov V, Mitin V and Stroscio M A 1995 *Phys. Rev. B* **51** 9930
[6] Nishiguchi N, Ando Y and Wybourne M 1997 *J. Phys.: Condens. Matter* **9** 5751
[7] Balandin A A and Wang K L 1998 *Phys. Rev. B* **58** 1544
[8] Balandin A A and Wang K L 1998 *J. Appl. Phys.* **84** 6149
[9] Khitun A, Balandin A A and Wang K L 1999 *Superlattices Microstruct.* **26** 181
[10] Zou J and Balandin A A 2001 *J. Appl. Phys.* **89** 2932
[11] Mingo N 2003 *Phys. Rev. B* **68** 113308
[12] Mingo N and Yang L 2003 *Phys. Rev. B* **68** 245406
[13] Zincenco N D, Nika D L, Pokatilov E P and A. A 2007 *J. Phys.: Conf. Ser.* **92** 012086
[14] Aksamija Z and Knezevic I 2010 *Phys. Rev. B* **82** 045319
[15] Cocemasov A I and Nika D L 2012 *J. Nanoel. Optoel.* **7** 370
[16] Crismari D V and Nika D L 2012 *J. Nanoel. Optoel.* **7** 701
[17] Cocemasov A I, Nika D L, Fomin V M, Grimm D and Schmidt O G 2015 *Appl. Phys. Lett.* **107** 011904
[18] Li D, Wu Y, Kim P, Shi L, Yang P and Majumdar A 2003 *Appl. Phys. Lett.* **83** 2934
[19] Liu W and Ashegi M 2006 *J. Heat Transfer* **128** 75
[20] Boukai A I, Bunimovich Y, Tahir-Kheli J, Yu J K, Goddard III W A and Heath J R 2008 *Nature* **451** 168
[21] Hochbaum A I, Chen K, Delgado R D, Liang W, Garnett E C, Najarian M, Majumdar A and Yang P 2008 *Nature* **451** 163
[22] Wingert M C, Kwon S, Hu M, Poulikakos D, Xiang J and Chen R 2015 *Nano Lett.* **15** 2605
[23] Zhao Y, Yang L, Kong L, Nai M H, Liu D, Wu J, Liu Y, Chiam S Y, Chim W K, Lim C T, Li B, Thong J T L and Hippalgaonkar K 2017 *Adv. Funct. Mater.* **27** 1702824
[24] Pokatilov E P, Nika D L and Balandin A A 2003 *Superlattices Microstruct.* **33** 155
[25] Pokatilov E P, Nika D L and Balandin A A 2004 *Appl. Phys. Lett.* **85** 825
[26] Pokatilov E P, Nika D L and Balandin A A 2005 *Phys. Rev. B* **72** 113311
[27] Nika D L, Pokatilov E P and Balandin A A 2008 *Appl. Phys. Lett.* **93** 173111
[28] Nika D L, Zincenco N D and P. E 2009 *J. Nanoel. Optoel.* **4** 180
[29] Nika D L, Pokatilov E P, Balandin A A, Fomin V M, Rastelli A and Schmidt O G 2011 *Phys. Rev. B* **84** 165415
[30] Hu M, Giapis K P, Goicochea J V, Zhang X and Poulikakos D 2011 *Nano Lett.* **11** 618
[31] Wingert M C, Chen Z C Y, Dechaumphai E, Moon J, Kim J H, Xiang J and Chen R 2011 *Nano Lett.* **11** 5507
[32] Nika D L, Cocemasov A I, Isacova C I, Balandin A A, Fomin V M and Schmidt O G 2012 *Phys. Rev. B* **85** 205439
[33] Bi K, Wang J, Wang Y, Sha J, Wang Z, Chen M and Chen Y 2012 *Phys. Lett. A* **376** 2668
[34] Hu M and Poulikakos D 2012 *Nano Lett.* **12** 5487
[35] Nika D L, Cocemasov A I, Crismari D V and Balandin A A 2013 *Appl. Phys. Lett.* **102** 213109
[36] Benisty H, SotomayorTorrès C M and Weisbuch C 1991 *Phys Rev B* **44** 10945
[37] Murdin B N, Heiss W, Langerak C J G M, Lee S C, Galbraith I, Strasser G, Gornik E, Helm M and Pidgeon C R 1997 *Phys. Rev. B* **55** 5171
[38] Heitz R, Born H, Guffarth F, Stier O, Schliwa A, Hoffmann A and Bimberg D 2001 *Phys. Rev. B* **64** 241305
[39] Inoue K and Matsuno T 1993 *Phys. Rev. B* **47** 3771
[40] Tsuchiya T and Ando T 1993 *Phys. Rev. B* **48** 4599
[41] Zianni X, Simserides C and Triberis G 1997 *Phys. Rev. B* **55** 16324
[42] Pokatilov E P, Nika D L, Askerov A S and Balandin A A 2007 *J. App. Phys.* **102** 054304
[43] Pokatilov E P, Nika D L and Balandin A A 2004 *J. Appl. Phys.* **95** 5626
[44] Pokatilov E P, Nika D L and Balandin A A 2006 *Appl. Phys. Lett.* **89** 113508
[45] Fonoberov V A and Balandin A A 2006 *Nano Lett.* **6** 2442
[46] Kargar F, Debnath B, Kakko J P, Sainatjoki A, Lipsanen H, Nika D L, Lake R K and Balandin A A 2016 *Nat. Comm.* **7** 13400
[47] Novoselov K S, Geim A K, Morozov S V, Jiang D, Zhang Y, Dubonos S V, Grigorieva I V and Firsov A A 2004 *Science* **306** 666
[48] Zhang Y, Tan Y W, Stormer H L and Kim P 2005 *Nature* **438** 201
[49] Nair R R, Blake P, Grigorenko A N, Novoselov K S, Booth T J, Stauber T, Peres N M R and Geim A K 2008 *Science* **320** 1308
[50] Mak K F, Shan J and Heinz T F 2011 *Phys. Rev. Lett.* **106** 046401
[51] Balandin A A, Ghosh S, Bao W, Calizo I, Teweldebrhan D, Miao F and Lau C 2008 *Nano Lett.* **8** 902
[52] Balandin A A 2011 *Nat. Mat.* **10** 569
[53] Nika D L and Balandin A A 2017 *Rep. Prog. Phys.* **80** 36502
[54] Ghosh S, Calizo I, Teweldebrhan D, Pokatilov E P, Nika D L, Balandin A A, Bao W, Miao F and Lau C N 2008 *Appl. Phys. Lett.* **92** 151911.
[55] Bolotin K I, Sikes K J, Jiang Z, Klima M, Fudenberg G, Hone J, Kim P and Stormer H L 2008 *Solid State Commun.* **146** 351
[56] Hong X, Posadas A, Zou K, Ahn C H and Zhu J 2009 *Phys. Rev. Lett.* **102** 136808
[57] Cai W, Moore A L, Zhu Y, Li X, Chen S, Sh L and Ruoff R S 2010 *Nano Lett.* **10** 1645

[58] Jauregui L A, Yue Y, Sidorov A N, Hu J, Yu Q, Lopez G, Jalilian R, Benjamin D K, Delk D A, Wu W, Liu Z, Wang X, Jiang Z, Ruan X, Bao J, Pei S S and Chen Y P 2010 *ECS Trans.* **28** 73

[59] Chen S, Wu Q, Mishra C, Kang J, Zhang H, Cho K, Cai W, Balandin A A and Ruoff R S 2012 *Nat. Mater.* **11** 203

[60] Li H, Ying H, Chen X, Nika D L, Cocemasov A I, Cai W, Balandin A A and Chen S 2014 *Nanoscale* **6** 13402

[61] Dorgan V E, Behnam A, Conley H J, Bolotin K I and Pop E 2013 *Nano Lett.* **13** 4581

[62] Seol J H, Jo I, Moore A L, Lindsay L, Aitken Z H, Pettes M T, Li X, Yao Z, Huang R, Broido D, Mingo N, Ruoff R S and Shi L 2010 *Science* **328** 213

[63] Nika D L, Pokatilov E P, Askerov A S and Balandin A A 2009 *Phys. Rev. B* **79** 155413

[64] Lindsay L, Broido D and Mingo N 2010 *Phys. Rev. B* **82** 115427

[65] Lindsay L, Li W, Carrete J, Mingo N, Broido D A and Reinecke T L 2014 *Phys. Rev. B* **89** 155426

[66] Klemens P G 2000 *J. Wide Bandgap Mater.* **7** 332

[67] Klemens P G 2001 *Int. J. Thermophys.* **22** 265

[68] Nika D L, Ghosh S, Pokatilov E P and Balandin A A 2009 *Appl. Phys. Lett.* **94** 203103

[69] Nika D L, Askerov A S and Balandin A A 2012 *Nano Lett.* **12** 3238

[70] Fugallo G, Cepellotti A, Paulato L, Lazzeri N, Marzari N and Mauri F 2014 *Nano Lett.* **14** 6109

[71] Munoz E, Lu J and Yakobson B I 2010 *Nano Lett.* **10** 1652

[72] Jiang J W, Wang J S and Li B 2009 *Phys. Rev. B* **79** 205418

[73] Jang Y Y, Cheng Y, Pei Q X, Wang C W and Xiang Y 2012 *Phys. Lett. A* **376** 3668

[74] Park M, Lee S C and Kim Y S 2013 *J. Appl. Phys.* **114** 053506

[75] Alofi A and Srivastava G P 2012 *J. Appl. Phys.* **112** 013517

[76] Alofi A and Srivastava G P 2013 *Phys. Rev. B* **87** 115421

[77] Ma F, Zheng H B, Sun Y J, Yang D, Xu K W and Chu P K 2012 *Appl. Phys. Lett.* **101** 111904

[78] Fthenakis Z G, Zhu Z and Tomanek D 2014 *Phys. Rev. B* **89** 125421

[79] Pereira L F C and Donadio D 2013 *Phys. Rev. B* **87** 125424

[80] Malekpour H, Ramnani P, Srinivasan S, Balasubramanian G, Nika D L, Mulchandani A, Lake R K and Balandin A A 2016 *Nanoscale* **8** 14608

[81] Shen Y, Xie G, Wei X, Zhang K, Tang M, Zhong J, Zhang G and Zhang Y W 2014 *J. Appl. Phys.* **115** 063507

[82] Feng T and Ruan X 2018 *Phys. Rev. B* **97** 045202

[83] Jang W, Chen Z, Bao W, Lau C N and Dames C 2010 *Nano Lett.* **10** 3909

[84] Nika D L and Balandin A A 2012 *J. Phys.: Condens. Matter* **24** 233203

[85] Shahil K M F and Balandin A A 2012 *Nano Lett.* **12** 861

[86] Pop E, Varshney V and Roy A K 2012 *MRS Bull.* **37** 1273

[87] Sadeghi M, Pettes M T and Shi L 2012 *Solid State Commun.* **152** 1321

[88] Wermhoff A P 2012 *Int. J. Transp. Phenom.* **13** 121

[89] Renteria J D, Nika D L and Balandin A A 2014 *Appl. Sci.* **4** 525

[90] Malekpour H and Balandin A A 2018 *J. Raman Spectrosc.* **49** 106

[91] Ghosh S, Bao W, Nika D L, Subrina S, Pokatilov E P, Lau C N and Balandin A A 2010 *Nat. Mater.* **9** 555

[92] Ghosh S, Nika D L, Pokatilov E P and Balandin A A 2009 *New J. Phys.* **11** 095012

[93] Judek J, Gertych A P, Świniarski M, Łapinska A, Dużyńska A and Zdrojek M 2015 *Sci. Rep.* **5** 12422

[94] Vallabhaneni A K, Singh D, Bao H, Murthy J and Ruan X 2016 *Phys. Rev. B* **93** 125432

[95] Li Q Y, Xia K, Zhang J, Zhang Y, Li Q, Takashi K and Zhang X 2017 *Nanoscale* **9** 10784

[96] Jo I, Pettes M T, Lindsay L, Ou E, Weathers A, Moore A L and Shi L 2015 *AIP Advances* **5** 053206

[97] Jeong J Y, Lee K M, Shrestha R, Horne K, Das S, Choi W, Kim M and Choi T Y 2016 *Mater. Res. Express* **3** 055004

[98] Liu J, Wang T, Xu S, Yuan P, Xu X and Wang X 2016 *Nanoscale* **8** 10298

[99] Pettes M T, Jo I, Yao Z and Shi L 2011 *Nano Lett.* **11** 1195

[100] Jang W, Bao W, Ling L, Lau C N and Dames C 2013 *Appl. Phys. Lett.* **103** 133102

[101] Wang Z, Xie R, Bui C T, Liu D, Ni X, Li B and Thong J T L 2011 *Nano Lett.* **11** 113

[102] Cocemasov A I, Nika D L and Balandin A A 2013 *Phys. Rev. B* **88** 035428

[103] Nika D L, Cocemasov A and Balandin A A 2014 *Appl. Phys. Lett.* **105** 031904

[104] Cocemasov A I, Nika D L and Balandin A A 2015 *Nanoscale* **7** 12851

[105] Limbu T B, Hahn K R, Mendoza F, Sahoo S, Razink J J, Katiyar R S and Morell G 2017 *Carbon* **117** 367

[106] Kuang Y, Lindsay L and Huang B 2015 *Nano Lett.* **15** 6121

[107] Zhan H, Zhang Y, Bell J M and Gu Y 2015 *J. Phys. Chem. C* **119** 1748

[108] Shen X, Wang Z, Wu Y, Liu X, He Y B and Kim J K 2016 *Nano Lett.* **16** 3585

[109] Si C, Lu G, Cao B Y, Wang X D, Fan Z and Feng Z H 2017 *J. Appl. Phys.* **121** 205102

[110] D'Souza R and Mukherjee S 2017 *Phys. Rev. B* **95** 085435

[111] Li L H and Chen Y 2016 *Adv. Funct. Mater.* **26** 2594

[112] Jo I, Pettes M T, Kim J, Watanabe K, Taniguchi T, Yao Z and Shi L 2013 *Nano Lett.* **13** 550

[113] Zhou H, Zhu J, Liu Z, Yan Z, Fan X, Lin J and Tour J M 2014 *Nano Res.* **7** 1232

[114] Wang C, Guo J, Dong L, Aiyiti A, Xu X and Li B 2016 *Sci. Rep.* **6** 25334

[115] Sichel E K, Miller R E, Abrahams M S and Buiocchi C J 1976 *Phys. Rev. B* **13** 4607

[116] Lindsay L and Broido D A 2011 *Phys. Rev. B* **84** 155421

[117] Mak K F, Lee C, Hone J., Shan J and F. T 2010 *Phys. Rev. Lett.* **105** 136805

[118] Radisavljevic B, Radenovic A, Brivio J, Giacometti I V and Kis A 2011 *Nat. Nanotechnol.* **6** 147

[119] Yan R, Simpson J R, Bertolazzi S, Brivio J, Watson M, Wu X and Xing H G 2014 *ACS Nano* **8** 986

[120] Jo I, Pettes M T, Ou E, Wu W and Shi L 2014 *Appl. Phys. Lett.* **104** 201902

[121] Taube A, Judek J, Łapiníska A and Zdrojek M 2015 *ACS Appl. Mater. Interfaces* **7** 5061

[122] Cai Y, Lan J, Zhang G and Zhang Y W 2014 *Phys. Rev. B* **89** 035438

[123] Ding Z, Jiang J W, Pei Q X and Zhang Y 2015 *Nanotechnology* **26** 065703

[124] Ding Z, Pei Q X, Jiang J W and Zhang Y W 2015 *J. Phys. Chem. C* **119** 16358

[125] Gu X, Li B and Yang R 2016 *J. Appl. Phys.* **119** 085106

[126] Liu J, Choi G M and Cahill D G 2014 *J. Appl. Phys.* **116** 233107

[127] Li L, Yu Y, Ye G J, Ge Q, Ou X, Wu H and Zhang Y 2014 *Nat. Nanotechnol.* **9** 372

[128] Xia F, Wang H and Jia Y 2014 *Nat. Commun.* **5** 4458

[129] Koenig S P, Doganov R A, Schmidt H, Castro Neto A H and Özyilmaz B 2014 *Appl. Phys. Lett.* **104** 103106

[130] Ong Z Y, Cai Y, Zhang G and Zhang Y W 2014 *J. Phys. Chem. C* **118** 25272

[131] Zhu L, Zhang G and Li B 2014 *Phys. Rev. B* **90** 214302

[132] Xu W, Zhu L, Cai Y, Zhang G and Li B 2015 *J. Appl. Phys.* **117** 214308

[133] Luo Z, Maassen J, Deng Y, Du Y, Garrelts R P, Lundstrom M S and Xu X 2015 *Nat. Commun.* **6** 8572

[134] Hong Y, Zhang J, Huang X and Zeng X C 2015 *Nanoscale* **7** 18716

[135] Liu T H and Chang C C 2015 *Nanoscale* **7** 10648.

[136] Qin G, Yan Q B, Qin Z, Yue S Y, Hu M and Su G 2015 *Phys. Chem. Chem. Phys.* **17** 4854

[137] Jain A and McGaughey A J 2015 *Sci. Rep.* **5** 8501

[138] Zhang Y Y, Pei Q X, Jiang J W, Wei N and Zhang Y W 2016 *Nanoscale* **8** 483

[139] Liu X, Gao J, Zhang G and Zhang YW 2017 *Adv. Funct. Mater.* **27** 1702776

[140] Jang H, Wood J D, Ryder C R, Hersam M C and Cahill D G 2015 *Adv. Mater.* **27** 8017

[141] Kang J S, Ke M and Hu Y 2017 *Nano Lett.* **17** 1431

[142] Lee S, Yang F, Suh J, Yang S, Lee Y, Li G and Park J 2015 *Nat. Commun.* **6** 8573

[143] Smith B, Vermeersch B, Carrete J, Ou E, Kim J, Mingo N, Akinwande D and Shi L 2017 *Adv. Mater.* **29** 1603756